

# Through thickness fatigue strength variation in thick S460 plates

Anis Mohabeddine <sup>1,2</sup>, Koen Creusen <sup>3</sup>, Jasper Winkes <sup>3</sup>,

José A.F.O. Correia <sup>4</sup>, Milan Veljkovic <sup>1</sup>

<sup>1</sup> Faculty of Civil Engineering and Geosciences, Delft University of Technology, the Netherlands, email: a.i.mohabeddine@tudelft.nl

<sup>2</sup> Faculty of Engineering, University of Porto, Portugal

<sup>3</sup> C1 Connections, the Hague, the Netherlands

<sup>4</sup> INEGI & CONSTRUCT, Faculty of Engineering, University of Porto, Portugal

Steel thick plates (i.e. thickness > 80 mm) are increasingly used in wind turbine offshore structures. The fracture toughness of thick plates is well addressed in the literature; however, little is known on their fatigue resistance. Thick plates exhibit distinct features that can present additional structural integrity issues compared to conventional thin steel plates, caused by the significant plane strain effects, heterogeneous through-thickness micro structures and mechanical properties, and inherent larger material defects. This paper presents a comparison between the fatigue resistance of two distinct regions in a 100 mm thick steel slab, namely, the surface region and the core region. High cycle fatigue experimental tests are performed under force-controlled condition for both regions using dog-bone small-scale specimens. Large material defects are observed in the core region. The fatigue results of surface specimen show longer fatigue life compared to core specimens. Large scatter of the data is present in core specimens due to the presence of large voids. The fracture patterns of the different specimens are identified through light and scanning microscopy. Statistical analysis of the fatigue data is conducted, and a fatigue *S-N* curve is derived when applicable.

*Keywords: Fatigue, high-strength steel, thick steel slabs, defects, statistical evaluation, S-N curves*

## 1 Introduction

High-strength steel slabs with a thickness over 100 mm are increasingly used in offshore structures and bridge construction. Despite their growing importance and their established presence in the market, published independent research on the characterisation of the mechanical and fatigue behavior of thick high strength steel remains very limited.

S460 steel is widely used in structural applications where high strength, toughness, and weldability are required. The advanced thermo-mechanical controlled processing (TMCP) is crucial for thick sections, allowing even low-alloy steels to achieve a remarkable balance of strength and toughness [1]. The low carbon content and fine-grained microstructure offer significant benefits, particularly improved weldability and enhanced toughness [2]. These attributes are essential for offshore wind turbines construction, as the standards' requirements are very high. Offshore wind turbine steel support structure can be exposed to demanding service conditions, where localized defects can significantly affect the structural integrity. Due to size effects the presence of manufacturing defects in thick sections is more likely, making it crucial to address their influence.

To the best knowledge of the authors, research on the fatigue of thick steel base material is very limited in the literature. Some fatigue data on moderately thick butt-welded steel plates (i.e. thickness  $\leq 120$  mm) can be found in the literature [3]. These data were the basis for the derivation of the empirical formula to account for size effects in butt welded joint in Eurocode 3 part 1-9 [4]. Although this is based on large database, only a few tests with thick steel plates are included, see [3]. Nowadays, thick steel plates  $\geq 100$  mm can be found in the market and are adopted in the designs of the new generation of tall wind turbines [5]. Igwemezie et al. [2] identified several key structural integrity issues related to thick plates, including significant plane strain effects, heterogeneous through-thickness microstructures, mechanical property variations across the thickness, and inherent material defects. Some research addresses the microstructure [6], [7] monotonic behaviour [8] and fracture toughness [9], but fatigue research thick plates remain scarce. As part of OFWEC 3 research project, Mohabeddine et al. [10] showed that there is a considerable variation of the mechanical properties across the thickness of the plate. The surface region of a 100 mm thick TMPC steel plate exhibited a 15% higher average yield stress and 8% higher ultimate stress compared to the core region of the plate. The hardness tests showed a significant gradient that correlates well with the variation of the yield and ultimate stress. The core

region has relatively larger grains and a lower texture compared to the surface region of the plate. The presence of porosity in the core region was very noticeable. This might have significant impact on the fatigue properties as will be discussed later in this paper.

This paper presents the results of an experimental study on the fatigue properties of thick high-strength steel (S460) manufactured with a thermomechanical controlled process. A steel plate of 100 mm thickness is considered for this purpose. Fatigue test on coupon specimens meticulously extracted from the core and the near surface regions of the plate is conducted. A comparison between the fatigue performance of the two distinct regions is presented. Analysis of the fracture surfaces and identification of the different failure patterns is presented. Statistical analysis of the data and derivation of S-N curves is presented. A comparison with fatigue tests on conventional thin S460 from the literature is also presented.

## **2 Material and experimental details**

The present study is part of the OFWEC 3 research project, which encompasses a large experimental investigation, including several microstructural, mechanical, and fatigue tests. This paper focuses on the fatigue of small-scale specimens extracted from two distinct regions of a thick plate, namely the core situated in the core and the near surface region.

### **2.1 Material**

Fined grained high strength TMCP steel (S460 MLO) with a thickness of 100 mm is investigated in this study. The plate received a heat treatment process to relieve residual stresses from thermomechanical rolling. The heat treatment steps consist of heating up to 300 °C with a free rate, then 160 °C/hr up to 600 °C ± 10 °C, holding for 200 min, cooling with 200 °C/hr until 300 °C, and finally free air cooling. Before the delivery, the plates received a series of inspections including destructive and non-destructive tests. This includes chemical composition tests, Charpy, hardness, and ultrasonic testing. The material certificate shows that the average tensile test results conducted according to ISO 6892-1 (B) meet the minimum requirements of EN 10225-1 [11], where the yield strength = 452 MPa, the ultimate strength = 555 MPa and the elongation after fracture is = 27%. The hardness tests HV10 at room temperature reported a mean value of 250 and Charpy tests according to ISO 148-1 with an average of 418 J at -40 °C which exceeds the minimum requirement of

60 J of offshore structures. The chemical composition of the material, as presented in the material certificate, is presented in Table 1. The carbon equivalent (CE) content according to the formula adopted in EN-10225-1:19 [11] is also presented:

$$CE = C + MN/6 + (CR + MO + V)/5 + (NI + CU)/15 \quad (1)$$

Table 1. Chemical composition

C	SI	MN	P	S	N	CU	MO
0.059	0.213	1.49	0.013	0.0006	0.0030	0.250	0.166
0.044	0.213	1.50	0.013	0.0006	0.0034	0.252	0.165
NI	CR	V	NB	$\eta$	B	CE	
0.445	0.053	0.001	0.020	0.003	0.0003	0.40	
0.445	0.054	0.000	0.019	0.003	0.0002	0.38	

Additional test conducted by the authors [10] showed the core region of the plate exhibits on average a yield stress and an ultimate stress of 453 MPa and 555 MPa, respectively. Whereas the surface region exhibits on average a yield stress and an ultimate stress of 525 MPa and 601 MPa, respectively.

## 2.2 Geometry and manufacturing specifications of the specimens

As the focus of this study is to investigate the fatigue performance of thick plates and identify the difference between the core and the surface region, the specimens were meticulously extracted from these two distinct regions as defined in Figure 1.

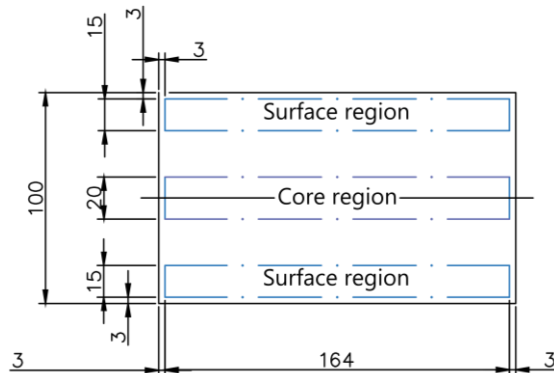


Figure 1. Location of the core and surface regions considered

Figure 2 provides a schematic representation of the fatigue specimens. Core and surface specimens are designated by the letters 'C' and 'S', respectively. The geometry of these specimens meets the requirements ISO-1099 [5]. The specimens design ensures a uniform distribution of stress in the gauge length and minimizes the stress concentration factor (SCF = 1.04) at the radius, as confirmed via the finite element analysis (results not shown for brevity). The specimens were produced perpendicular to the rolling direction. A surface roughness of  $R_a \leq 2 \mu\text{m}$  was achieved in all specimens.

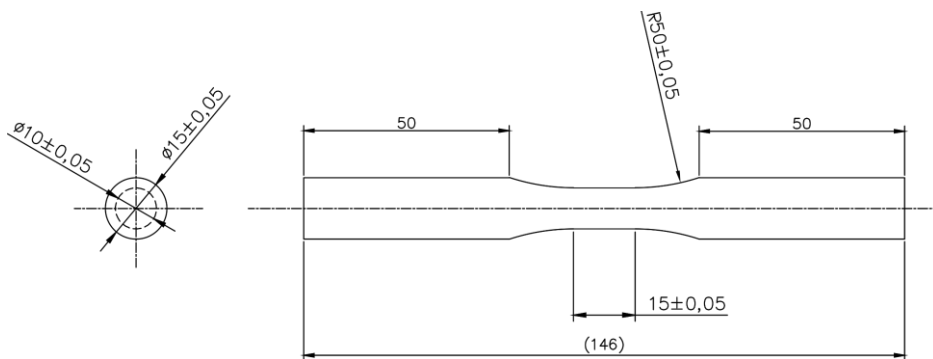


Figure 2. Fatigue specimens geometrical and manufacturing specifications

### 2.3 Experimental program and instrumentation

Fatigue tests were performed according to ISO-1099 standard [12] under force-controlled conditions. Instron 1251 test machine, as shown in Figure 3, with a 100 kN capacity is used for this purpose and each test was carried out until complete failure of the specimen. The experimental matrix included 20 specimens each for the core and surface regions. Tests were conducted at a stress ratio  $R = 0$  and a frequency of 40 Hz was adopted. The first tests were started with a maximum stress level close to the experimentally observed monotonic yield strength, and for the next tested specimens, the stress range



Figure 3. Instron 1251 fatigue dynamic machine

was progressively reduced or increased by 20 MPa increments depending on the number of cycles to failure observed. After  $10^7$  cycles, the tests were stopped and considered as runouts. For cases close to the fatigue limit, smaller steps of 10 MPa were applied. Most of the stress range values were tested with at least two repetitions to increase the reliability of the results.

### 3 Fatigue life results and statistical analysis

#### 3.1 Qualitative analysis of the data

The fatigue data of the tested specimens are presented in the Appendix. Tests with number of cycles without failure  $N \geq 10^7$  are considered as run-outs and are indicated in the subsequent figures by an arrow attached to the test result symbol. Figure 4 shows the fatigue data of specimens from the surface and the core regions. Clearly, the surface specimens show a higher fatigue resistance. The core specimens show a large scatter where it seems that the data can be divided into two subgroups that follow distinct linear curves, as shown in the figure. The data that follow line A show a fatigue resistance slightly lower than surface specimens. The core specimens that are in line with line B exhibit relatively very low fatigue resistance. This is due to the presence of a defect as will be shown in the subsequent section.

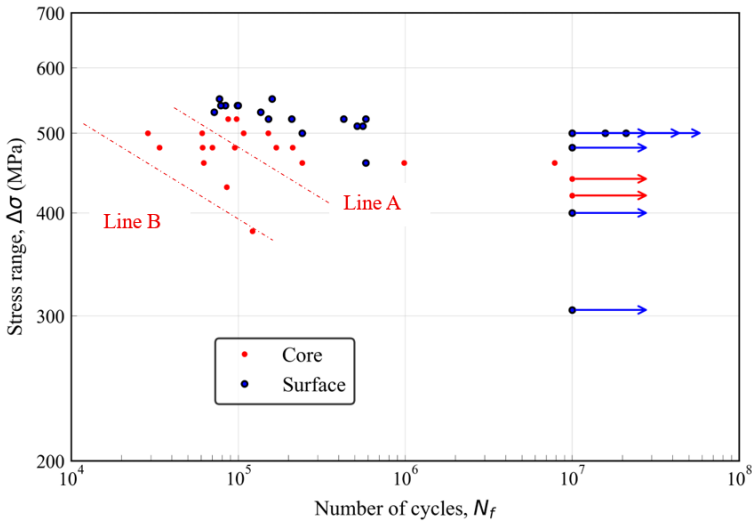


Figure 4. Fatigue data of core and surface specimens

### 3.2 Statistical analysis and fatigue S-N curves

This section presents the statistical analysis of the fatigue data and the derivation of constant amplitude fatigue S-N curves, following the recommendations by DNV-RP-C203 [13], Schneider and Maddox [14], and ISO 12107 [15]. The methodology primarily involves deriving a fitted mean curve that best captures the trend of the experimental results and evaluating the variability of the data relative to this mean curve. A characteristic design curve can be proposed based on a tolerable probability of failure, as recommended by the relevant design code. The influence of overloads in the high cycle regime is beyond the scope of this study; only constant amplitude loading is considered. The logarithm of the number of cycles “log(N)” is treated as the dependent variable and the logarithm of the stress range “log( $\Delta\sigma$ )” is the independent variable. The fitting is conducted using the maximum likelihood method assuming a 75% confidence. The linear relationship between log( $\Delta\sigma$ ) and log(N) is known to hold only within certain stress ranges [14], [16]–[18]. Thus, only data within a defined range can be used to estimate the best-fit linear mean S-N curve. This range lies between the low-cycle fatigue region and the point where data start to approach the fatigue limit. For non-welded details, it is common practice to exclude data after 2 million cycles as they start to converge to a fatigue limit after this point [14]. In this study, the fitted mean S-N curves are derived only from data that are between  $10^4 \leq N \leq 2 \times 10^6$  cycles, excluding runouts. To ensure a more accurate fitting, a test of linearity is performed, and the influence of outliers are assessed. The characteristic design S-N curves are derived under the assumption that the fatigue data follow a normal distribution, with the design curve providing a 97.7% probability of survival at 75% confidence, as recommended in DNV-RP- C203 [13].

The mean curve is fitted using the following procedure:

- a. Calculate the coefficient of correlation, shown in Eq. 1, to measure the strength and direction of the linear relationship between the variables log(N) and log( $\Delta\sigma$ ).

$$\text{Corr}(X, Y) = \frac{\text{Cov}(X, Y)}{S_y S_x} \quad (1)$$

where:

$$\text{Cov}(X, Y) = \frac{1}{n-1} \sum_{i=1}^n (y_i - \bar{y})(x_i - \bar{x}) \quad (2)$$

and  $x_i$  are the observations of the independent variable and  $y_i$  of the dependent variable. The bar sign designates the sample mean. In fatigue data the  $y_i = \log(\Delta \sigma_i)$  and  $x_i = \log(N_i)$ . The parameters:  $S_x$  and  $S_y$  are the standard deviations of the two variables. The correlation coefficient is a normalized quantity with a value between  $-1 \leq \text{Corr}(X, Y) \leq 1$ . In a graphical representation of the correlation coefficient as shown in Figure 5 and Figure 6, the plot can be divided in 4 quadrants and each quadrants illustrate the sign of relationship between  $X$  and  $Y$ .

- b. Plot the graphical representation of the coefficient of covariance and check linear relationship of the variables.
- c. Fit the mean curve using the maximum likelihood method.
- d. Conduct a t-test to check the validity of the linear relationship between the two variables.

Assess the influence of outliers using the Cook's distance test.

Figure 5 illustrates the correlation coefficient for the surface specimens, the data show a negative relationship between the two variables which is expected in fatigue problems. Some of the data are quite close to the mean lines which indicate a low strength of the linear relationship between the variables. This can be confirmed by looking at the parameters  $\text{Corr}$ ,  $R^2$  and the  $P$ -value shown in Table 5. Cook's distance is a way to identify points that negatively affect the regression model. The measurement is a combination of each observation's leverage and residual values; the higher the leverage and residuals, the

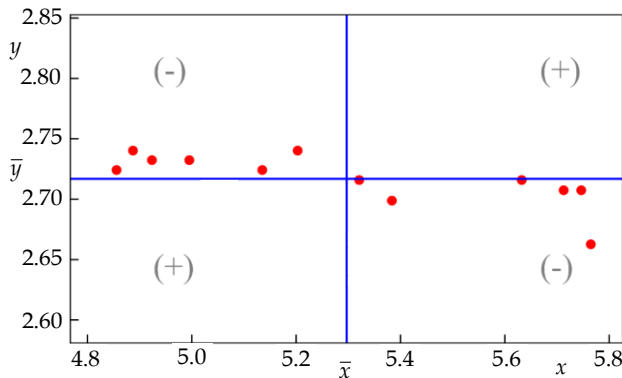


Figure 5. Graphical illustration of the correlation coefficient (Surface specimens)

higher the Cook's distance. If the Cook's distance for a given point is higher than  $3(k+1)/n$ , so it is highly influential. The parameter  $k$  is the number of independent variables and  $n$  is the size of the sample. Figure 7 shows the Cook's distance test for surface specimens, where clearly there are no data points that are highly influential however some of them show a higher distance than the other which explains the relatively low  $R^2$  obtained.

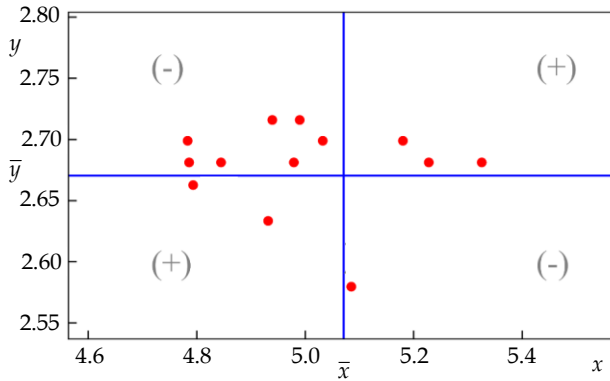


Figure 6. Graphical illustration of the correlation coefficient (Core specimens)

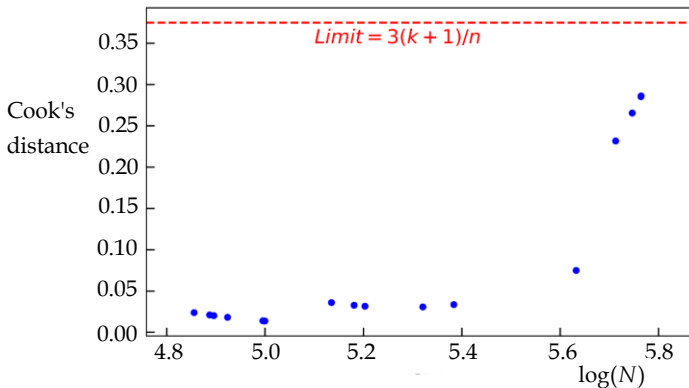


Figure 7. Cook's distance (surface specimens)

Figure 6 illustrates the correlation coefficient for the core specimens. Notably, 5 out of 13 data points lie in the positive quadrant, which is counterintuitive, as in fatigue  $\log(N)$  and  $\log(\Delta\sigma)$  are expected to have an inverse relationship, resulting in a negative slope. The calculated correlation coefficient is very low,  $Corr = -0.206$ , indicating a lack of correlation and suggesting that a linear relationship is not present. Consequently, performing linear regression analysis on this dataset would be inappropriate. While removing outliers is a

common method to refine data for analysis, nearly 40% of the points (5 out of 13) qualify as outliers, making this approach unfeasible. As a result, deriving a mean *S-N* curve for this dataset is not possible. The significant scatter in the data is attributed to the presence of defects in the core specimens, which are considerable in size compared to the cross-sectional area of these small-scale specimens. Note these specimens are not representative of a full thick plate, where the cross-sectional area is much larger, and the impact of such defects is less pronounced. When defects are as such significant, the fatigue crack propagation is more appropriate. Note, if small structural details are machined out of thick plates that contain similar defects, it is expected that the fatigue resistance will be considerably poor.

Table 2 presents the statistical and the fatigue *S-N* curves parameters for both surface and core specimens (if applicable). This includes the coefficient of correlation (*Corr*), the *R* squared parameter which is a goodness of fit measure for the linear regression model, and the *P*-value of the *t*-test to check the validity of the linear relationship between the response and predictor variables. The smaller the corresponding *P*-value, the stronger the linear relationship between the variables. The slope *m* is provided for both the mean and the characteristic curves. The parameter  $\log(a)$  represents the *Y*-intercept of the mean *S-N* curve and  $\Delta\sigma_c$  is the stress range at  $2 \times 10^6$  cycles of the characteristic curve. Figure 8 illustrates the fatigue data and characteristics curves for surface specimens, the parameters of the characteristic curve are the slope *m* and  $\Delta\sigma_c$  for every set of specimens.

Table 2. Statistical parameters of the mean *S-N* curves

	Mean curve					Char. curve		
	<i>Corr.</i>	<i>m</i>	$\log(a)$	<i>R</i> <sup>2</sup>	<i>P</i> -value	Relationship	<i>m</i>	$\Delta\sigma_c$ [MPa]
Surface	-0.722	12.40	39.01	0.52	0.0016	Linear	12.41	387
Core	-0.206	n.a.	n.a.	n.a.	n.a.	Not linear	n.a.	n.a.

### 3.3 Comparison with data from the literature and fatigue design codes

Figure 9 presents the fatigue data of this study together with some fatigue data collected from a the database made by Boller and Seeger [19]. The data include mainly STE 460 steel which is the German name for S460 and one North American steel grade equivalent to

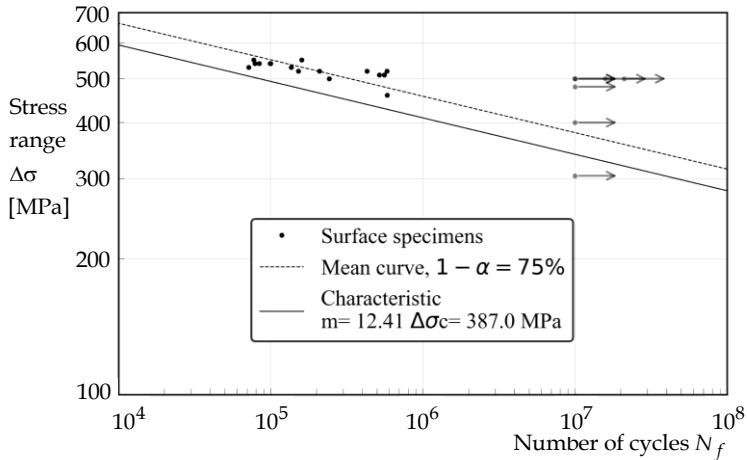


Figure 8. Characteristic design curve for surface specimens

S460 TMCP. WSTE is also and S460 made with TMCP and the remaining are either normalized or as received. Note the data was taken from test under reversed cycle loading  $R = -1$ , so the presented data was normalized to  $R = 0$  using the methodology prescribed in DNV-RP-C203. The data of surface specimens lay between the scatter of the fatigue data from the literature, while core specimens fatigue data show the lowest performance. The fatigue characteristic  $S-N$  curve proposed for surface specimen is not above the data with

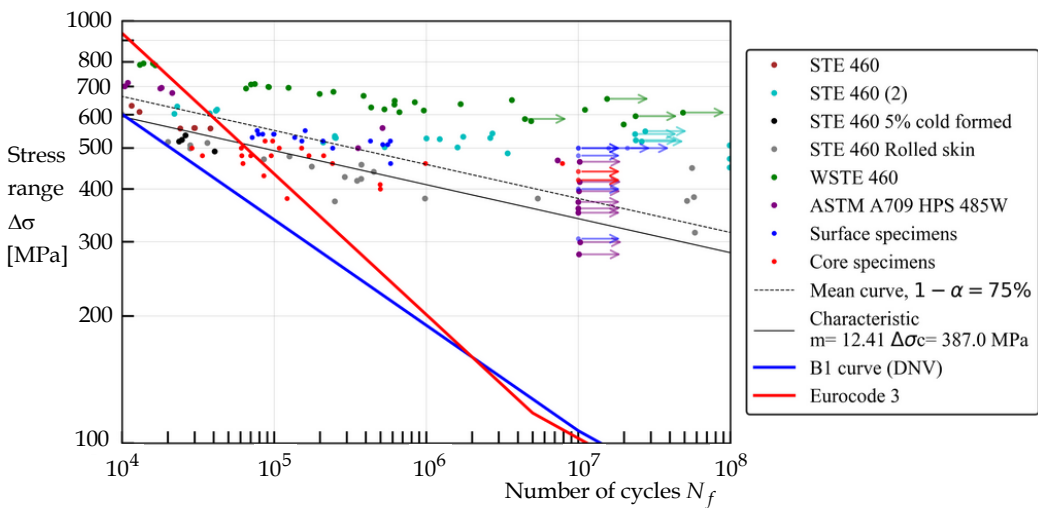


Figure 9. Comparison between the fatigue data of this study and fatigue data from the literature [19] as well as the Eurocode and DNV base material  $S-N$  curves

rolled skin or that received cold forming. The Eurocode 3 base material design curve seems to be not conservative at high stress ranges whereas the DNV curve represent a lower limit for all the data.

#### 4 Fracture surface of fatigue specimens

The fracture surface of the fatigue specimens was analysed using visual inspection, light microscopy and electron scanning microscopy (SEM). The visual inspection is conducted to initially identify approximately the different zones of the fracture surface including (crack initiation sites, crack propagation, and fracture) and to isolate specimens and areas of most interest for further microanalysis.

An example of visual inspection is shown in Figure 10, where Figure 10 (a) shows the fracture surface of a core specimen "F-C-02-400-" that failed due to the presence of a large void which deserves lot of attention, and Figure 10 (b) illustrates a surface specimen with no visible defects. For both specimens, the crack seems to start from the surface or from a defect and propagate towards the centre until final fracture.



a) Core specimen failed due to large defect

b) Surface specimen failed without visible defect

Figure 10. Visual inspection of the fracture surface of a core specimen featuring a visible defect and surface specimen without a defect

The Keyence VHX-X1 digital microscope was used for the light microscopy. Figure 11 shows the fracture surface of specimen "F-S-64-520-1," a representative surface specimen. River markings indicate the crack initiation site on the top left image. The top images

reveal a rough, flat surface typical of stage II stable fatigue crack propagation, as well as a teared region with large river markings typical of stage III rapid crack propagation and complete fracture. Reflective spots, highlighted in the red boxes near the surface, suggest areas of brittle failure, possibly indicative of intergranular decohesion near the surface of the specimen. The bottom right image shows a higher magnification of the shiny spots, where a grain seems to appear. Overall, the specimen exhibited a fatigue failure typical of ductile metals, the shiny spot did not penalise the fatigue life, as the specimen showed a long fatigue life before failure. Figure 8 shows the fracture surface of a core specimen (F-C-64-500-1) that features two bands of initial defects that appears as lamellar of voids. The authors believe that these are clusters of voids that appears in a lamellar form. The remaining fatigued surface is relatively small with some ratchet marks perpendicular to the void. Figure 13 shows the fracture surface of another core specimen (F-C-64-500-2) that features a relatively smaller defect of the same nature of the one observed in Figure 8. River marks show clearly that the crack initiated around the defect. Ratchet marks suggest

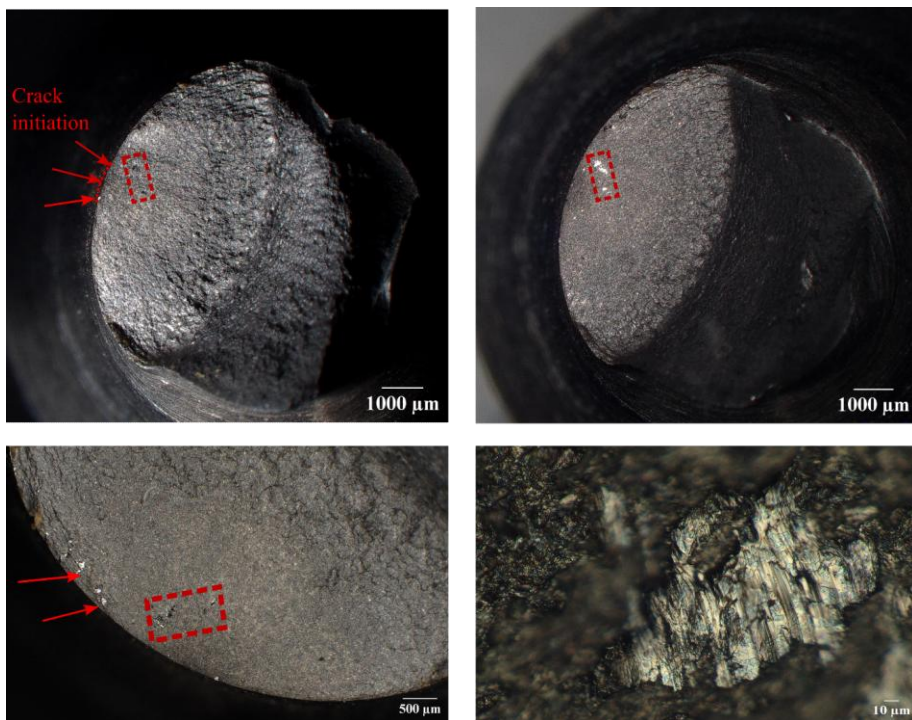


Figure 11. fracture surface of F-S-64-520-1

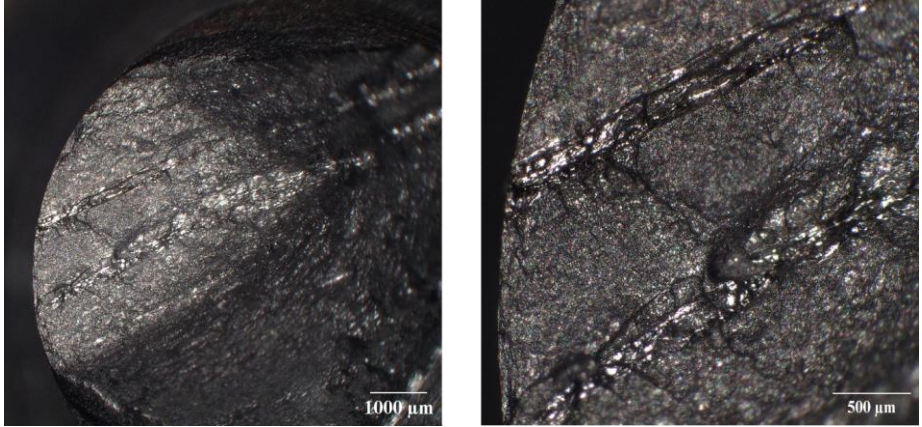


Figure 12. Fracture surface of F-C-64-500-1

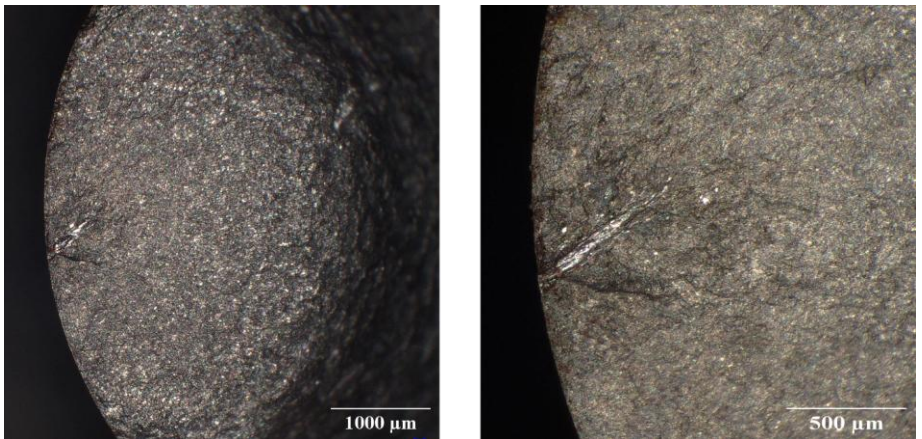


Figure 13. Fracture surface of F-C-64-500-2

that different crack initiation sites around the defect. The flat fracture surface typically of stage II crack propagation appears to be larger than the specimen in Figure 8, which confirms the longer fatigue life.

The SEM was conducted on OL JXA 8900R microprobe using an electron beam with energy of 10 keV and beam current of 200 nA employing Wavelength Dispersive Spectrometry (WDS). From Figure 14, SEM micrograph with 90× magnification is shown for a specimen that failed from a large defect. The fatigue crack initiation process started around or within the defect. Looking at the area around the void next to the edge of the specimen, the surface morphology features elongated, wavy striations, micro-voids, and some dimples,

which could suggest ductile tearing or localized shear deformation. These features may be a result of material plasticity, influenced by stress concentration raised by the shape of the voids. At the void, the surface is smooth without any sign of striations due to fatigue loading, some grain boundaries are apparent. The river patterns suggest that the crack propagated towards the edge of the specimen and in radial direction towards the centre of the cross-sectional area. Generally, the fracture surfaces exhibited the typical mechanisms associated with the fatigue failure of metallic materials, such as the river patterns, traces of plastic deformation, and ductile dimples.

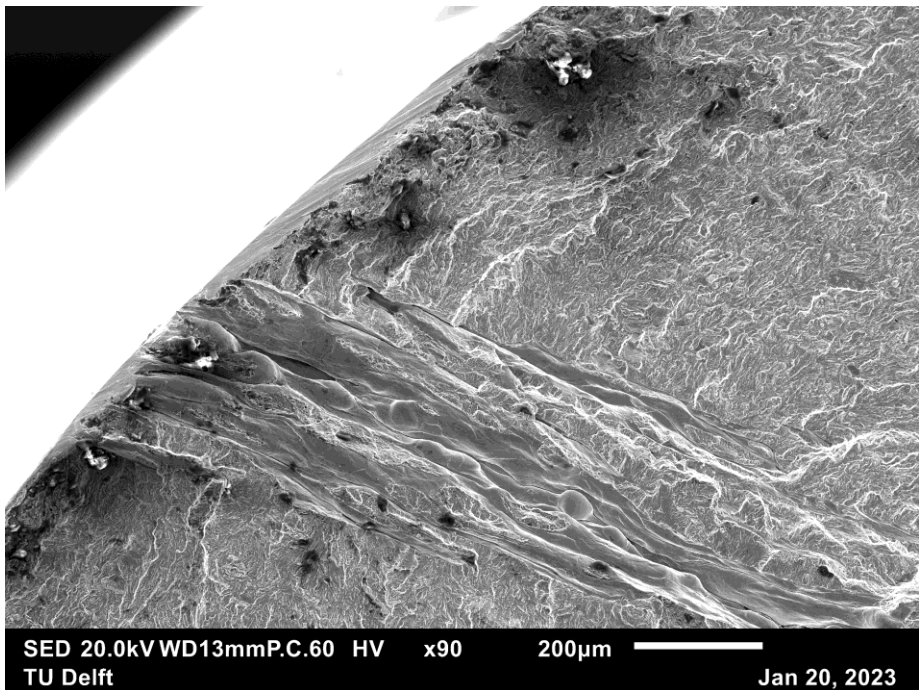


Figure 14. Electron microscopy of a crack initiation sites at a defect

## 5 Conclusion

This paper presents an experimental study on the high cycle fatigue of the thick high strength steel S460 manufactured using the thermomechanical controlled process. A steel plate of 100 mm thick is used for this purpose. high cycle fatigue tests are performed under force-controlled condition. Small scale specimens are made from two distinguished region

across the thickness of the plate, namely, the near surface region and the core region. The fatigue results of both regions are presented and analysed, where:

- The core specimens' results show a lower fatigue resistance compared to surface specimens as well as to all the data collected from the literature. A significant scatter was observed in the data for core specimens that is attributed to the presence of large defects, which are considerable in size compared to the cross-sectional area of these small-scale specimens. Note these specimens are not representative of a full thick plate, where the cross-sectional area is much larger, and the impact of such defects should be less pronounced. When the presence of defects is as such significant the fatigue crack propagation is more appropriate. However, if structural components are manufactured from thick plates with this conditions, the fatigue performance is expected to be quite poor.
- Evidence of fatigue crack initiation starting from defects in the core specimens was observed using light and scanning microscopy. River markings indicated clearly the crack initiation sites and propagation zones.
- Surface specimens achieve a higher fatigue performance and lower scatter compared to core specimens regardless the influence of defects which is due to the differences in the microstructure in terms of grain size and texture.
- A fatigue design curve is derived for surface specimens, whereas this was not possible for core specimens' data as the coefficient of correlation revealed no linear relationship between the stress range and the number of cycles in log-log scale.

### *Acknowledgements*

The authors express their sincere gratitude to the Rijksdienst voor Ondernemend Nederland for funding this research through the HER+-01217760 research grant.

## References

- [1] M. X. Xiong, P. W. Pi, W. Gong, M. F. Yang, and Z. F. Ou, "Mechanical properties of TMCP high strength steels with different strength grades at elevated temperatures," *J. Build. Eng.*, vol. 48, no. October 2021, p. 103874, 2022, doi: 10.1016/j.jobbe.2021.103874.
- [2] V. Igwemezie, A. Mehmanparast, and A. Kolios, "Current trend in offshore wind energy sector and material requirements for fatigue resistance improvement in large wind turbine support structures – A review," *Renew. Sustain. Energy Rev.*, vol. 101, no. October 2016, pp. 181–196, 2019, doi: 10.1016/j.rser.2018.11.002.
- [3] M. M. Pedersen, "Thickness Effect in Fatigue of Welded Butt Joints: A Review of Experimental Works," *Int. J. Steel Struct.*, vol. 19, no. 6, pp. 1930–1938, 2019, doi: 10.1007/s13296-019-00254-y.
- [4] European Committee for Standardization (CEN), "Eurocode 3: Design of steel structures - Part 1-9: Fatigue," 2005.
- [5] T. Lehnert and T. Graf, "New developments in heavy plates for offshore structures," *ce/papers*, vol. 6, no. 3–4, pp. 1129–1132, Sep. 2023, doi: 10.1002/cepa.2493.
- [6] V. Bertolo et al., "A comprehensive quantitative characterisation of the multiphase microstructure of a thick-section high strength steel," *J. Mater. Sci.*, vol. 57, no. 13, pp. 7101–7126, 2022, doi: 10.1007/s10853-022-07121-y.
- [7] Q. Wang, Q. Ye, Z. Wang, L. Kan, and H. Wang, "Thickness effect on microstructure, strength, and toughness of a quenched and tempered 178 mm thickness steel plate," *Metals (Basel)*, vol. 10, no. 5, pp. 1–16, 2020, doi: 10.3390/met10050572.
- [8] N. Yang, C. Su, X. F. Wang, and F. Bai, "Research on damage evolution in thick steel plates," *J. Constr. Steel Res.*, vol. 122, pp. 213–225, 2016, doi: 10.1016/j.jcsr.2016.03.014.
- [9] V. A. Popovich and I. M. Richardson, "Fracture toughness of welded thick section high strength steels and influencing factors," *TMS Annu. Meet.*, no. March 2015, pp. 1031–1038, 2015, doi: 10.1002/9781119093466.ch125.
- [10] A. Mohabeddine, "Base material fatigue testing 077-003," Delft, 2023.
- [11] EN 10225, "Weldable structural steels for fixed offshore structures – Technical delivery conditions."
- [12] ISO1099, *Metallic materials - Fatigue testing - Axial force-controlled method*. 2017.
- [13] DNVGL-RP-C203, "Fatigue design of offshore steel structures," 2021.
- [14] C. Schneider and S. J. Maddox, "Best Practice Guide on Statistical Analysis of Fatigue Data," Apr. 2002.

- [15] ISO 12107, "Metallic materials – Fatigue testing – Statistical planning and analysis of data - ISO 12107," Test, p. 13, 2003.
- [16] A. Mohabeddine et al., "An approach for predicting fatigue life of cfrp retrofitted metallic structural details," *Int. J. Fatigue*, p. 106557, 2021, doi: 10.1016/j.ijfatigue.2021.106557.
- [17] A. Mohabeddine, J. Correia, P. Aires Montenegro, A. De Jesus, J. Miguel Castro, and F. Berto, "Probabilistic S-N curves for CFRP retrofitted steel details," *Int. J. Fatigue*, vol. 148, 2021, doi: 10.1016/j.ijfatigue.2021.106205.
- [18] J. KOHOUT and S. VECHET, "A new function for fatigue curves characterization and its multiple merits," *Int. J. Fatigue*, vol. 23, no. 2, pp. 175–183, Jan. 2001, doi: 10.1016/S0142-1123(00)00082-7.
- [19] C. Boller and T. Seeger, *Materials Data for Cyclic Loading Part A: Unalloyed Steels*, vol. V. Amsterdam: Elsevier, 1987.

## Appendix

Table 3. Experimental fatigue tests of specimens

Test number	Location in the plate	Stress range [MPa]	Cycles to failure
F-C-02-520-1	Core	520	8.69E+04
F-C-02-520-2		520	9.77E+04
F-C-02-500-1		500	1.51E+05
F-C-02-500-2		500	1.08E+05
F-C-64-500-1		500	2.87E+04
F-C-64-500-2		500	6.07E+04
F-C-02-480-1		480	6.11E+04
F-C-02-480-2		480	1.69E+05
F-C-02-480-3		480	2.11E+05
F-C-64-480-1		480	7.00E+04
F-C-64-480-2		480	3.37E+04
F-C-64-480-3		480	9.53E+04
F-C-02-460-1		460	7.84E+06
F-C-02-460-2		460	6.21E+04
F-C-64-460-1		460	9.86E+05
F-C-02-440-1		440	1.00E+07*
F-C-02-440-2		440	1.00E+07*
F-C-02-430-1		430	8.54E+0
F-C-02-420-1		420	>1.00E+7*
F-C-02-420-2		420	>1.00E+7*
F-C-02-410-1	410	4.96E+05	
F-C-02-400-1	400	4.99E+05	
F-C-02-380-1	380	1.22E+5	
F-S-02-550-1	Surface	550	7.71E+04
F-S-02-550-2		550	1.59E+05
F-S-02-540-1		540	8.38E+04
F-S-02-540-2		540	9.89E+04
F-S-64-540-1		540	9.98E+04
F-S-64-540-2		540	7.86E+04

F-S-02-530-1	530	1.36E+05
F-S-02-530-2	530	7.17E+04
F-S-02-520-1	520	2.09E+05
F-S-02-520-2	520	4.29E+05
F-S-64-520-1	520	5.81E+05
F-S-64-520-1	520	1.52E+05
F-S-02-510-1	510	5.16E+05
F-S-02-510-2	510	5.57E+05
F-S-02-500-1	500	>1.00E+07*
F-S-02-550-2	500	>1.00E+07*
F-S-02-550-3	500	2.42E+05
F-S-64-500-1	500	>2.10E+07*
F-S-64-305-1	500	>1.58E+07*
F-S-02-480-1	460	5.81E+05
F-S-02-460-1	480	>1.00E+07*
F-S-02-400-1	400	>1.00E+07*
F-S-02-305-1	305	>1.00E+07*

---

Note: the superscript (\*) indicates that test is considered as a runout.